Submitted to

Global Biogeochemical Cycles

Supporting Information for

Constraining global marine iron source and scavenging fluxes with GEOTRACES dissolved iron measurements in an ocean biogeochemical model

Christopher J. Somes[1], Andrew W. Dale[1], Klaus Wallmann[1], Florian Scholz[1], Wanxuan Yao[1], Andreas Oschlies[1], Juan Muglia[2], Andreas Schmittner[3], Eric P. Achterberg[1]

[1] GEOMAR Helmholtz Centre for Ocean Research Kiel, 24105 Kiel, Germany

[2] Centro para el Estudio de los Sistemas Marinos, CONICET, 2915 Boulevard Brown, U9120ACD, Puerto Madryn, Argentina

[3] College of Earth, Ocean, and Atmospheric Sciences, Oregon State University, Corvallis, Oregon 97331, USA

Corresponding author: Christopher J. Somes (csomes@geomar.de)

Contents of this file

Introduction

This section documents minor changes made from previously published versions (Somes et al., 2017;Muglia et al., 2017) that were applied to all model simulations in this study. The core model code is based on the Model of Ocean Biogeochemistry and Isotopes (MOBI), version 2.0 (https://github.com/OSU-CEOAS-Schmittner/UVic2.9), which is based on the University of Victoria (UVic) Earth System Model of intermediate complexity (Eby et al., 2013;Weaver et al., 2001).

Text S1. Physical Model

We applied the background vertical mixing setup from Somes et al. (2017) to the default MOBI 2.0 version. This setup applies background vertical mixing of 0.15 $cm^2\ s^{-1}$ in the ocean interior consistent with open ocean microstructure observations (Fischer et al., 2013), which caused a reduction in the large-scale overturning and an underestimation of $\Delta^{14}C$ values. In order to reinvigorate the large-scale circulation, we increased the tidal mixing efficiency parameter to 0.28 (from 0.2), applied a background horizontal diffusivity of 20 $m^2\ s^{-1}$, and increased the atmospheric moisture diffusivity in the Southern Ocean by 20% (e.g. Muglia & Schmittner (2015)), all of which contributed to an improved representation of $\Delta^{14}C$ (Figure S1).

Text S2. Marine Biogeochemical Model

Since MOBI version 2.0 integrated the latest improvements to the nitrogen (Somes and Oschlies, 2015), carbon chemistry (Kvale et al., 2015), and iron (Muglia et al., 2017), minor parameter changes were made to achieve a best fit to nutrient distribution (Figure S1, Table S1). Other structural changes are documented below.

The production of semi-refractory dissolved organic matter (DOM) has been modified to now include an additional source term from the remineralization of particulate organic matter (POM), along with phytoplankton mortality that previous versions Somes & Oschlies (2015) used. This new term represents DOM production by heterotrophic bacteria as they respire POM. The two DOM production factors have similar spatial patterns, but with the bacterial term based on POM remineralization extending to greater depths. The production fraction parameters (see Table S1) were chosen so they represent roughly equivalent total DOM production rate when integrated over the global ocean, and that they produce surface DON concentrations that are consistent with observations (Figure S2).

We have modified the low oxygen threshold including the reduction of dissolved iron (DFe) scavenging in the model. This parameterization was implemented to account for elevated DFe concentrations that exist in low oxygen waters associated with redox cycling including high nitrite concentrations, although it remains unclear exactly what processes contribute to these elevated low oxygen DFe concentrations (Moffett et al., 2015). Previous model versions applied a sharp threshold gradient at the dissolved O_2 concentration 5 mmol m^{-3} (Figure S3). However, elevated DFe only exists in lower dissolved O_2 concentrations <~2 mmol m^{-3}, so in this study we apply a function that has a sharper gradient at lower dissolved O_2 concentrations (red line in Figure S3) using the equation $\tanh(\kappa \cdot O_2)$ where κ=0.25.

Sedimentary carbon oxidation (C_{ox}) has been modified in all simulations following the Niemeyer et al. (2017) implementation of Flögel et al. (2011). This scheme estimates carbon oxidation from the difference between sinking particulate flux entering the sediment and burial. It has been constructed using a global compilation of sedimentary data that shows higher carbon burial efficiency, and thus lower carbon oxidation in continental margins ($\mathrm{Burial}=0.14 \cdot RR_{POC}^{1.11}$) compared to the deep-sea ($\mathrm{Burial}=0.014 \cdot RR_{POC}^{1.05}$) sediments. Instead of applying an abrupt transition at 1000 meters depth as in Niemeyer et al. (2017) between these surface and deep sea systems, we applied a linear transition to the numerator and exponent coefficients from 500 meters to 1500 meters. Note that previous model marine iron versions (e.g. Nickelsen et al. (2015); Muglia et al. (2017)) applied the temperature-dependent water column remineralization rate to organic matter sinking into sediments to estimate carbon oxidation in the sediments which does not capture the sedimentary carbon dynamics shown in Flögel et al. (2011).

Table S1. Marine Ecosystem-Biogeochemistry Parameters

Parameter	***Symbol***	***Value***	***Units***
Phytoplankton			
Initial slope of P-I curve	α	0.1	$(W\ m^{-2})^{-1}\ d^{-1}$
Photosynthetically active radiation	PAR	0.43	-
Light attenuation in water	k_w	0.04	m^{-1}
Light attenuation through phytoplankton	k_c	0.03	$m^{-1}(mmol\ m^{-3})^{-1}$
Light attenuation through sea ice	k_i	5	m^{-1}
NO_3 uptake half-saturation	k_{NO3}	0.7	$mmol\ m^{-3}$
PO_4 uptake half-saturation	k_{PO4}	0.044	$mmol\ m^{-3}$
DOP assimilation handicap	h_{DOP}	0.5	
minimum Fe uptake half-saturation	k_{Femin}	0.05	$nmol\ m^{-3}$
maximum Fe uptake half-saturation	k_{Femax}	0.5	$nmol\ m^{-3}$
Maximum growth rate (at 0°C)	a_0	0.6	d^{-1}
Phytoplankton fast-recycling rate (at 0°C)	$\mu_{P_O}0$	0.001	d^{-1}
Phytoplankton specific mortality rate	υ_{P_O}	0.03	d^{-1}
Calcifying Phytoplankton (P_C)			
Maximum growth rate (at 0°C)	a_0	0.3	d^{-1}
$CaCO_3$:POC production ratio	$R_{CaCO3:POC}$	0.065	0.065
NO_3 uptake half-saturation	k_{NO3}	0.35	$mmol\ m^{-3}$
PO_4 uptake half-saturation	k_{PO4}	0.022	$mmol\ m^{-3}$
minimum Fe uptake half-saturation	k_{Femin}	0.025	$nmol\ m^{-3}$
maximum Fe uptake half-saturation	k_{Femax}	0.25	$nmol\ m^{-3}$
Diazotrophic Phytoplankton (P_D)			

Parameter	***Symbol***	***Value***	***Units***
Diazotroph growth handicap	h_{P_D}	0.07	-
Fe uptake half-saturation	k_{Fe}	0.16	nmol m^{-3}
Diazotroph fast-recycling rate (at 0°C)	$\mu_{P_D 0}$	0.004	d^{-1}
Diazotroph specialist grazing rate	υ_{P_D}	0.7	d^{-1}
Diazotroph NO_3 uptake threshold	U_{NO3}	5	mmol m^{-3}
Zooplankton (Z)			
Assimilation efficiency	γ	0.7	
Maximum grazing rate (at 0°C)	g_Z	0.5	d^{-1}
Growth efficiency	ϖ	0.6	
Mortality	m_z	0.02	d^{-1}
Grazing preference P_O	Ψ_{P_O}	0.26	
Grazing preference P_D	Ψ_{P_D}	0.04	
Grazing preference P_C	Ψ_{P_C}	0.26	
Grazing preference Z	Ψ_Z	0.18	
Grazing preference D	Ψ_D	0.26	
Grazing half-saturation	k_{graz}	0.15	mmol N m^{-3}
Detritus (D)			
Remineralization rate	μ_{D0}	0.07	d^{-1}
Sinking speed at surface	w_{D0}	20	m d^{-1}
Increase of sinking speed with depth	m_w	0.05	d^{-1}

Parameter	***Symbol***	***Value***	***Units***
E-folding temperature of biological rates	T_b	15.65	ºC
Dissovled Organic Matter			
phytoplankton DOM production factor	σ_{PDOM}	0.08	
bacterial DOM production factor	σ_{DDOM}	0.02	
DON remineralization rate (at 0°C)	λ_{DON0}	9.4E−6	d^{-1}
DOP remineralization rate (at 0°C)	λ_{DOP0}	1.9E−5	d^{-1}
Elemental Ratios			
Molar Oxygen:Nitrogen	$R_{O:N}$	11	
Molar Carbon:Nitrogen	$R_{C:N}$	7	
Molar Iron:Nitrogen	$R_{Fe:N}$	38.5	µmol Fe / mol N
Phytoplankton Nitrogen:Phosphorus	$R_{N:P_{P_O}}$	16	
Diazotroph Nitrogen:Phosphorus	$R_{N:P_{P_D}}$	28	
Detritus Nitrogen:Phosphorus	$R_{N:P_D}$	16	
Zooplankton Nitrogen:Phosphorus	$R_{N:P_Z}$	16	

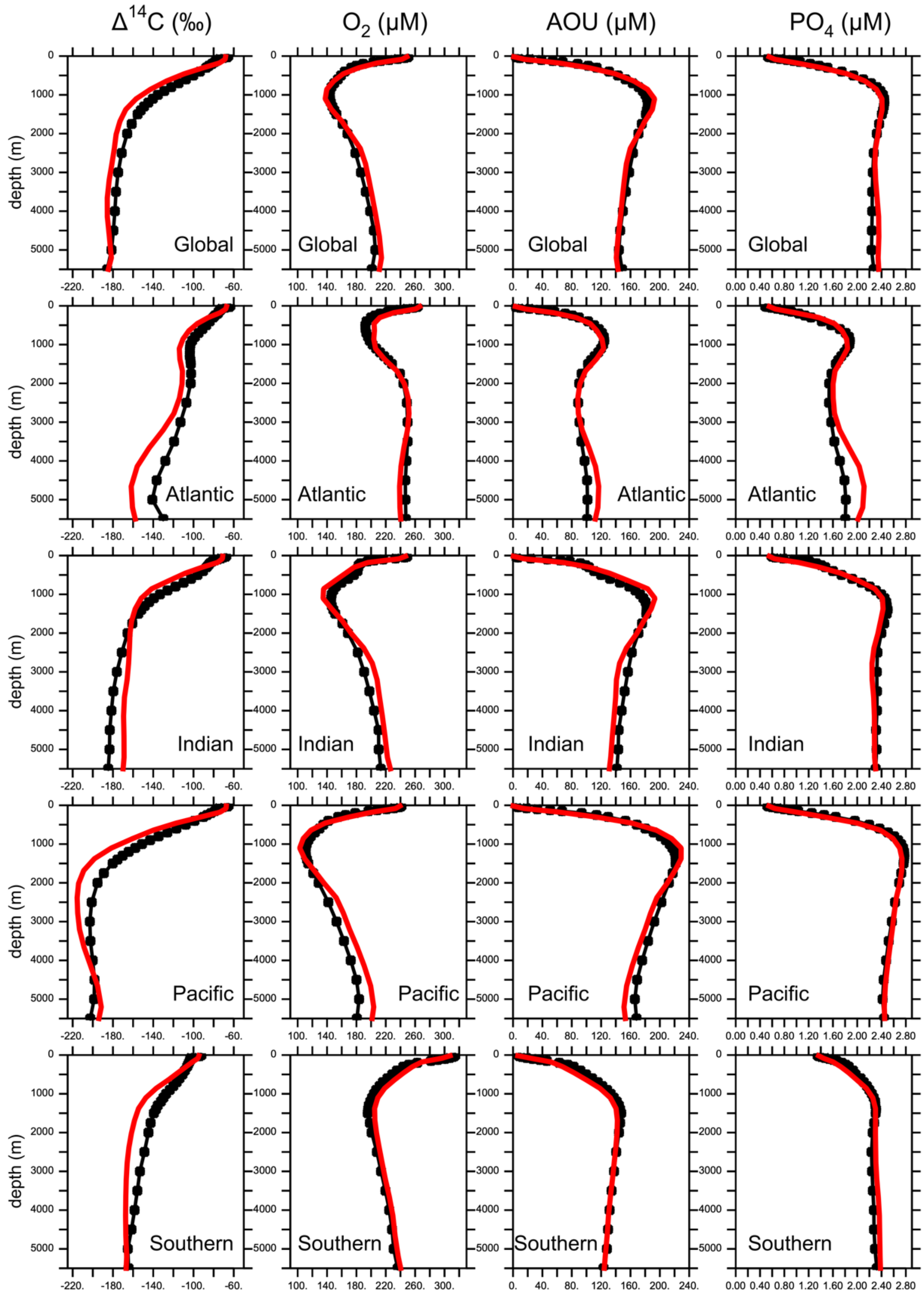
Δ14C (‰)
O2 (μM)
AOU (μM)
PO4 (μM)
depth (m)
Global
Atlantic
Indian
Pacific
Southern

Figure S1. Model-data comparison of basin scale average of radiocarbon ($\Delta^{14}C$) with GLODAP observations (Key et al., 2004) (left column), and dissolved oxygen (O_2), apparent oxygen utilization (AOU, center column), and phosphate (PO_4, right column) with World Ocean Atlas observations (Garcia et al., 2010a;Garcia et al., 2010b) (black circles) and the model simulation #5 *Atm+SedFeHigh_LigVar* (red lines).

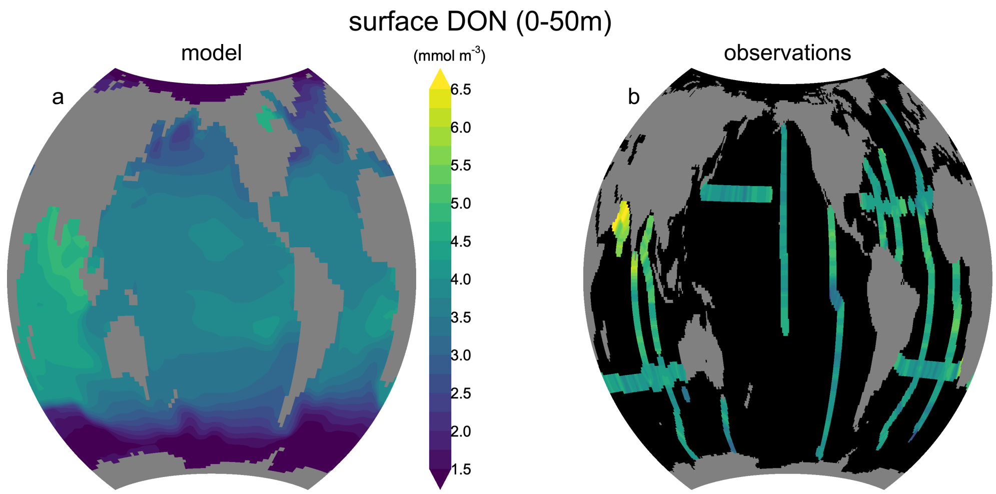

Figure S2. Surface (0-50 meters) dissolved organic nitrogen (DON) concentrations in the model simulation #5 *Atm+SedFeHigh_LigVar* and observations (Somes and Oschlies, 2015;Letscher et al., 2013). Note that the model only includes semi-refractory DON, whereas the observations include total DON.

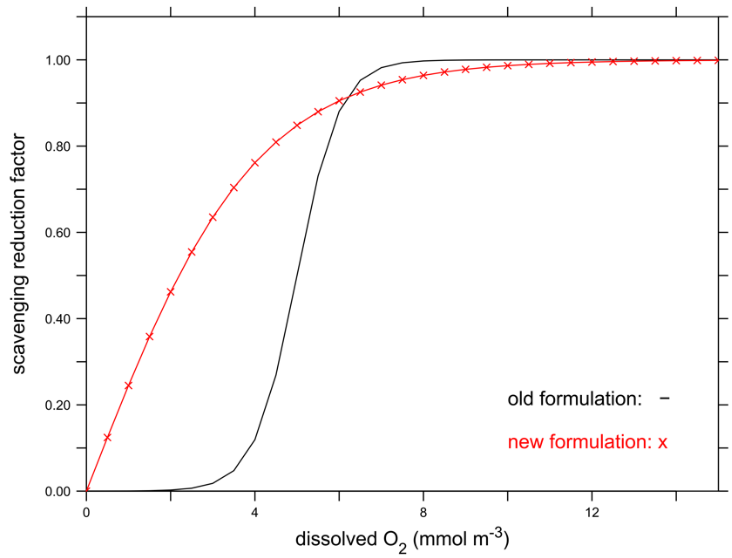

Figure S3. Modified function that reduces scavenging in oxygen deficient zones.

References

Eby, M., Weaver, A. J., Alexander, K., Zickfeld, K., Abe-Ouchi, A., Cimatoribus, A. A., Crespin, E., Drijfhout, S. S., Edwards, N. R., Eliseev, A. V., Feulner, G., Fichefet, T., Forest, C. E., Goosse, H., Holden, P. B., Joos, F., Kawamiya, M., Kicklighter, D., Kienert, H., Matsumoto, K., Mokhov, I. I., Monier, E., Olsen, S. M., Pedersen, J. O. P., Perrette, M., Philippon-Berthier, G., Ridgwell, A., Schlosser, A., Schneider von Deimling, T., Shaffer, G., Smith, R. S., Spahni, R., Sokolov, A. P., Steinacher, M., Tachiiri, K., Tokos, K., Yoshimori, M., Zeng, N., and Zhao, F.: Historical and idealized climate model experiments: an intercomparison of Earth system models of intermediate complexity, Clim. Past, 9, 1111-1140, 10.5194/cp-9-1111-2013, 2013.

Fischer, T., Banyte, D., Brandt, P., Dengler, M., Krahmann, G., Tanhua, T., and Visbeck, M.: Diapycnal oxygen supply to the tropical North Atlantic oxygen minimum zone, Biogeosciences, 10, 5079-5093, 10.5194/bg-10-5079-2013, 2013.

Flögel, S., Wallmann, K., Poulsen, C. J., Zhou, J., Oschlies, A., Voigt, S., and Kuhnt, W.: Simulating the biogeochemical effects of volcanic CO2 degassing on the oxygen-state of the deep ocean during the Cenomanian/Turonian Anoxic Event (OAE2), Earth and Planetary Science Letters, 305, 371-384, 10.1016/j.epsl.2011.03.018, 2011.

Garcia, H. E., Locarnini, R. A., Boyer, T. P., Antonov, J. I., Baranov, O. K., Zweng, M. M., and Johnson, D. R.: World Ocean Atlas 2009, Volume 3: Dissolved Oxygen, Apparent Oxygen Utilization, and Oxygen Saturation, in: NOAA Atlas NESDIS 70, edited by: Levitus, S., U.S. Government Printing Office, Washington, D.C., 344, 2010a.

Garcia, H. E., Locarnini, R. A., Boyer, T. P., Antonov, J. I., Zweng, M. M., Baranov, O. K., and Johnson, D. R.: World Ocean Atlas 2009, Volume 4: Nutrients (phosphate, nitrate, silicate), in: NOAA Atlas NESDIS 71, edited by: Levitus, S., U.S. Government Printing Office, Washington, D. C., 398, 2010b.

Key, R. M., Kozyr, A., Sabine, C. L., Lee, K., Wanninkhof, R., Bullister, J. L., Feely, R. A., Millero, F. J., Mordy, C., and Peng, T. H.: A global ocean carbon climatology: Results from Global Data Analysis Project (GLODAP), Global Biogeochemical Cycles, 18, GB4031, 10.1029/2004gb002247, 2004.

Kvale, K. F., Meissner, K. J., Keller, D. P., Eby, M., and Schmittner, A.: Explicit Planktic Calcifiers in the University of Victoria Earth System Climate Model, Version 2.9, Atmosphere-Ocean, 53, 332-350, 10.1080/07055900.2015.1049112, 2015.

Letscher, R. T., Hansell, D. A., Carlson, C. A., Lumpkin, R., and Knapp, A. N.: Dissolved organic nitrogen in the global surface ocean: Distribution and fate, Global Biogeochemical Cycles, n/a-n/a, 10.1029/2012GB004449, 2013.

Moffett, J. W., Vedamati, J., Goepfert, T. J., Pratihary, A., Gauns, M., and Naqvi, S. W. A.: Biogeochemistry of iron in the Arabian Sea, Limnology and Oceanography, 60, 1671-1688, 10.1002/lno.10132, 2015.

Muglia, J., and Schmittner, A.: Wind stress increases glacial atlantic overturning in climate models, Geophysical Research Letters, 42, 9862-9868, 10.1002/2015gl064583, 2015.

Muglia, J., Somes, C. J., Nickelsen, L., and Schmittner, A.: Combined Effects of Atmospheric and Seafloor Iron Fluxes to the Glacial Ocean, Paleoceanography, 32, 1204-1218, 10.1002/2016pa003077, 2017.

Nickelsen, L., Keller, D. P., and Oschlies, A.: A dynamic marine iron cycle module coupled to the University of Victoria Earth System Model: the Kiel Marine Biogeochemical Model 2 for UVic 2.9, Geoscientific Model Development, 8, 1357-1381, 10.5194/gmd-8-1357-2015, 2015.

Niemeyer, D., Kemena, T. P., Meissner, K. J., and Oschlies, A.: A model study of warming-induced phosphorus-oxygen feedbacks in open-ocean oxygen minimum zones on millennial timescales, Earth Syst. Dynam., 2017, 2, 357-367, 10.5194/esd-8-357-2017, 2017.

Somes, C., Schmittner, A., Muglia, J., and Oschlies, A.: A three-dimensional model of the marine nitrogen cycle during the Last Glacial Maximum constrained by sedimentary isotopes, Frontiers in Marine Science, 4, 10.3389/fmars.2017.00108, 2017.

Somes, C. J., and Oschlies, A.: On the influence of “non-Redfield” dissolved organic nutrient dynamics on the spatial distribution of N2 fixation and the size of the marine fixed nitrogen inventory, Global Biogeochemical Cycles, n/a-n/a, 10.1002/2014GB005050, 2015.

Weaver, A. J., Eby, M., Wiebe, E. C., Bitz, C. M., Duffy, P. B., Ewen, T. L., Fanning, A. F., Holland, M. M., MacFadyen, A., Matthews, H. D., Meissner, K. J., Saenko, O., Schmittner, A., Wang, H., and Yoshimori, M.: The UVic earth system climate model: Model description, climatology, and applications to past, present and future climates, Atmosphere-Ocean, 39, 361 - 428, 2001.